A case of 'mistaken identity': structurally similar ligand inhibits Thymidylate Kinase causing reversible filamentation of *E. coli*

Sanchari Bhattacharyya[a], Shimon Bershtein[b], Bharat V. Adkar[a], Jaie Woodard[a] and Eugene I. Shakhnovich[a*]

[a]Department of Chemistry and Chemical Biology, Harvard University, 12 Oxford St, Cambridge, MA 02138
[b]Department of Life Sciences, Ben-Gurion University of the Negev, POB 653, Beer-Sheva 8410501, Israel

*Correspondence should be addressed to E.I.S. (shakhnovich@chemistry.harvard.edu)

Abstract

Understanding genotype-phenotype relationship is a central problem in modern biology. Here we report that several destabilizing mutations in *E. coli* Dihydrofolate Reductase (DHFR) enzyme result in pronounced yet reversible filamentation of bacterial cells. We find that drop in DHFR activity in the mutants results in massive metabolic shifts leading to significant excess of dUMP and dCTP in the pyrimidine biosynthesis pathway. Both deoxyribonucleotides inhibit downstream essential enzyme Thymidylate Kinase (Tmk) which phosphorylates dTMP, eventually leading to almost complete loss of the DNA building block dTTP. Severe imbalance in deoxyribonucleotide levels ultimately leads to DNA damage, SOS response and filamentation. Supplementation of dTMP in the medium competitively alleviates Tmk inhibition and rescues filamentation, thereby illustrating a classic case of enzyme inhibition by structural mimic of its cognate ligand. Overall, this study highlights the complex interconnected nature of the metabolic network, and the fundamental role of folate metabolism in shaping the cell.

Introduction

Phenotype or fitness of microorganisms is often viewed in terms of different growth components, such as growth rate, duration of the lag phase, biomass yield at saturation, *etc*. However, the effect of mutations on cell morphology has received much less attention (Bollenbach et al., 2009; Monds et al., 2014). Microorganisms, most importantly bacteria, come in many different shapes and sizes, for example, rod-like, curved, helical, filamentous, round, flat sided, bean shaped, to name a few (Young, 2006). Despite this natural diversity, within a given species the shape remains surprisingly uniform, pointing towards the role of selection in 'shaping the bacteria' (Persat et al., 2014; Young, 2006). Moreover, several bacteria actively change their shape in response to changing environmental conditions (nutritional starvation (James et al., 1995; Pine and Boone, 1967; Ruoff, 1991), protection against predation by protists (Pernthaler, 2005), escape from immune cells (Champion and Mitragotri, 2006), or while going through different stages of the life-cycle. The best example of how bacterial shape contributes to virulence is exemplified by an uropathogenic *E. coli* that changes its shape from rod-like structures to 50μm-long filaments to resist phagocytosis and promote infection (Horvath et al., 2011; Justice et al., 2006).

Considering that cellular morphology has been important in microbial evolution, an important question is: How do mutations affect cell shape? The most common mutations that change cell shape and size are those associated with Fts family of proteins, which are directly involved in the formation of Z-ring during division (Addinall et al., 2005; Bi and Lutkenhaus, 1990; Pichoff et al., 2012). In *E. coli* and *B. subtilis*, studies have shown that mutations in peptidoglycan synthesis proteins (pbpA, rodA) (Ogura et al., 1989; Wei et al., 2003), and those in the bacterial mreBCD family of proteins (Kruse et al., 2003) disrupt cell shape by interfering with cell wall and cytoskeleton formation, respectively. Defects in chromosome partitioning have been shown to produce anucleate cells and cells of aberrant sizes (Hiraga et al., 1989). These studies focused on proteins directly involved in maintaining cell shape and divisions. However, mutations (or other loss of function such as inhibition by an antibiotic) in metabolic enzymes are also known to cause filamentation (Fonville et al., 2010; Sperber and Herman, 2017). A well-studied example is thymineless death (TLD) where cells acquire filamentous phenotype upon severe deprivation of essential metabolite thymine (Ahmad et al., 1998).

However, despite considerable effort, a mechanistic understanding of why bacterial cell shape can be sensitive to metabolic changes has been lacking.

In this work, we uncover that destabilizing mutations in the essential *E. coli* enzyme dihydrofolate reductase (DHFR) result in pronounced (>10 times of the normal cells) filamentation. DHFR catalyzes conversion of dihydrofolate to tetrahydrofolate, which is an essential one-carbon donor in purine, pyrimidine and amino acid biosynthesis pathways. Metabolomics analyses reveals that drop in DHFR activity in mutants leads to accumulation of metabolic precursors upstream in the pyrimidine biosynthesis pathway that, in turn, competitively inhibit another essential enzyme thymidylate kinase (Tmk), in a domino-like effect. Tmk phosphorylates dTMP (thymidine monophosphate) to dTDP, eventually to produce dTTP. As a result, severe imbalance in the concentrations of deoxyribonucleotide levels results in DNA damage, upregulation of SOS response, and filamentation. While triggered by dTTP loss, filamentation in mutant DHFR strains appears to be completely reversible under permissive conditions and differs from the characteristic thymineless death (Ahmad et al., 1998; Sangurdekar et al., 2010; Sangurdekar et al., 2011; Zaritsky et al., 2006). In fact, mutants in our study were found to phenotypically and metabolically resemble sub-MIC (sub-lethal) concentrations of trimethoprim (TMP) treatment that partially inhibits DHFR. Hence this phenomenon has important implications in tolerance, resistance and persistence of bacteria under sub-lethal doses of antibiotic treatment. Overall, this study highlights the pleiotropic nature of mutations and the complex connectivity of the metabolic network, where mutations can have “unintended” effects that extend far beyond its immediate metabolic vicinity.

Results

Several chromosomal mutations in folA gene give rise to slow growth and filamentation of E. coli

Earlier we reported that a group of highly destabilizing chromosomal DHFR mutations (W133V, V75H+I155A, I91L+W133V, and V75H+I91L+I155A) cause very slow growth of bacteria at 37°C and 42°C ((Bershtein et al., 2013; Bershtein et al., 2012) and Figure 1A). To understand the effects of these mutations on bacterial morphology, we grew those under two different growth conditions: M9 minimal media without and with supplementation with casamino acids (mixtures of all amino acids, except tryptophan, see *Methods*). In minimal media, median cell lengths of some mutants

(W133V and V75H+W133V at 42°C) were smaller compared to WT, while I91L+W133V (at 40°C) was marginally longer than WT (Figure 1B). Since the mutant cells grew much slower than WT, reduction in size was expected in accordance with the 'growth law' that shows a positive correlation between cell size and growth rate (Dai et al., 2018; Vadia and Levin, 2015). However, when M9 minimal medium was supplemented with amino acids, we found that cells carrying these mutations were pronouncedly filamentous. Figure 1C, D shows live cell DIC images of wild-type (WT) and I91L+W133V mutant DHFR strains at 30°C, 37°C, and 42°C, and DAPI staining of their nucleoids at 42°C (40°C for I91L+W133V strain). (See Supplementary Figure S1 for images of other low fitness mutant strains). In parallel to the detrimental effect of temperature on fitness, we noted that the morphologies were also temperature-sensitive. I91L+W133V and V75H+I91L+I155A strains exhibited a 1.5-1.75 fold increase (comparatively to WT) in the average cell length at 37°C (Figure 1E), while W133V and V75H+I155A were not elongated at 37°C. The latter, however, showed an increase up to 2.0-2.3 fold over WT cell lengths at 42°C (Figure 1F). Strains I91L+W133V and V75H+I91L+I155A showed 1.8-2.0 fold increase in the average cell length at 40°C, with some cells reaching up to 20μm in length (about 10 fold increase) (Figure S1). Besides temperature of growth, since filamentation was also strongly dependent on availability of amino acids in the growth medium, it seemed likely that it was the result of a metabolic response and not due to effect on the mutant DHFR proteins per se.

Filamentation is due to drop in DHFR activity

DHFR is a central metabolic enzyme that is involved in conversion of dihydrofolate to tetrahydrofolate, and the latter is an important 1-carbon donor in the biosynthesis of purines, pyrimidines, and certain amino acids like glycine and methionine. Earlier we had reported that fitness effects of the mutant DHFR strains was primarily due to very low abundance of the mutant proteins in the cell ((Bershtein et al., 2015; Bershtein et al., 2013) and Figure S2), an effect that could be rescued by deletion of Lon protease or by over-expressing chaperones like GroEL-ES (Bershtein et al., 2013). We, therefore, reasoned that filamentation could be a result of drop in DHFR activity in these cells. To confirm this, we supplemented the *E. coli* strains carrying chromosomal DHFR mutations with WT DHFR expressed from a plasmid and found that both filamentation (Figure 2A) and growth defects (Figure 2B) were fully rescued. On WT background, expression of extra DHFR resulted in some elongation, presumably due to toxicity of DHFR over-

expression (Bhattacharyya et al., 2016). We also found that plasmid expression of mutant proteins in WT cells did not result in any filamentation (Figure 2C) or growth defects (Figure 2D). This shows that filamentation is not due to toxicity of the mutant DHFR proteins.

Since filamentation is triggered by drop in DHFR activity, we hypothesized that treatment of WT cells with TMP, an antibiotic that targets bacterial DHFR, should also result in a similar phenotype. We treated WT *E. coli* cells with varying amounts of TMP at 37°C and 42°C. While we did observe filamentation and a drop in growth rates (Figure S3), cell length showed a non-monotonic dependence on TMP concentration at both temperatures (Figure S4 at 37°C, Figure 2E at 42°C). Cell length increased at low concentrations of TMP to reach a maximum at one-half of MIC (0.5μg/ml, MIC of TMP is 1μg/ml (Rodrigues et al., 2016; Tamer et al., 2019; Toprak et al., 2012)), and progressively decreased to 'no drug' levels at higher concentrations. This phenomenon is much more prominent at 42°C than 37°C, presumably because soluble DHFR amounts are lower at 42°C due to aggregation (Bershtein et al., 2012). Going a step ahead, we treated mutant DHFR strains with varying concentrations of TMP and found that filamentation steadily disappeared at higher concentrations of the drug (Figure 2F). It, therefore, seems that mutant DHFR strains mimic WT cells treated with sub-MIC levels of TMP. In other words, filamentation happens within a certain narrow range of the intracellular DHFR activity. Sequestration/loss of the entire pool of DHFR (which happens at much higher concentrations of TMP) presumably lead to growth arrest, while filamentation requires that the cell continues to synthesize its cellular mass, albeit poorer than WT.

Filamentous strains have imbalance between dTTP and other deoxyribonucleotides

Kwon et al (Kwon et al., 2010) have shown that inhibition of intracellular DHFR with very high concentration of TMP (6μg/ml) incurs large metabolic changes in the cell, with drop in glycine, methionine, purines and thymine levels. Similar data have been reported for engineered *E. coli* cells containing inactive mutants of DHFR (Rodrigues and Shakhnovich, 2019). However, as discussed in the previous section (Figure 2E), we found that cells treated with high concentrations of TMP were phenotypically (with regard to cell length) very different than those treated with sub lethal concentrations. Moreover, since presence of amino acids is crucial to obtaining the filamentous phenotype, detecting the metabolic changes under these conditions is central to understanding the processes that trigger cell filamentation. To that end, we carried out metabolomics analysis of

mutant strains under conditions of filamentation (in amino acid supplemented M9 medium at 42°C for WT and W133V and at 40°C for I91L+W133V) as well as under non-filamentation conditions (in minimal medium at 42°C for WT and W133V and at 40°C for I91L+W133V). In addition, we did similar analysis for WT cells treated with low TMP concentration (0.5μg/ml at 42°C, a condition that mimics phenotype of mutant strains and causes filamentation in the presence of amino acids) under both set of media conditions (with and without amino acids). We observed that in the absence of amino acids, mutant strains as well as TMP-treated WT exhibited very low levels of both purines and pyrimidines (Figure 3A shows levels relative to WT for I91L+W133V, while Figure S5A, B shows relative levels for W133V and WT+TMP, respectively; see Table S1 for data for all metabolites). Specifically, IMP levels were 5% of WT in W133V, 17% in I91L+W133V and 49% in TMP treated cells, while AMP levels were 47% of WT in W133V, 30% in I91L+W133V and 62% in TMP treated cells. In case of pyrimidines, dTMP levels were only 3% and 5% of WT levels in W133V and I91L+W133V, respectively, while dTTP levels in both were below the detection limit. Most amino acids showed large drop in abundance in mutant strains and following TMP treatment (Figure 3C for I91L+W133V; see Figure S5A, B for others). Surprisingly, many were not directly related to the folate biosynthesis pathway. Methionine and glycine biosynthesis require tetrahydrofolate derivatives, hence, expectedly, methionine levels were only 1-3% in mutant strains and 11% in TMP treated cells. However, in contrast to Kwon et al (Kwon et al., 2010), glycine levels were unaltered in mutant strains, and only dropped by 10% in TMP treated cells. Overall, we rationalize that large drop in methionine and purine (IMP) levels presumably stalls protein/RNA synthesis. Since increase in cell mass is essential for filamentation, cells under this condition are not filamented.

In the presence of 1% casamino acids, several but not all amino acids showed a marked increase in abundance (Figure 3D for I91L+W133V; see Figure S5 for others; see Table S1 for data for all metabolites). Methionine levels rose to 40% of WT levels for I91L+W133V mutant, while they increased much above WT levels for W133V strain and TMP-treated cells. Aspartate/asparagine, glutamine, histidine and tryptophan levels also showed a significant increase. Particularly interesting was the fact that purine levels were substantially rescued upon addition of amino acids (Figure 3B for I91L+W133V; see Figure S5A, B for others; see Figure S6 for metabolite concentrations as a function of time). IMP showed the maximal effect, increasing to 10-15 times over its levels in the absence of amino acids. ATP, ADP, AMP and GMP also showed

similar trends. Pyrimidine levels, in particular dTMP, also increased to 40-50% of WT levels. So, how does addition of amino acids lead to rescue of purine and pyrimidines despite low DHFR activity? We rationalize this observation in two possible ways. First, tetrahydrofolate, the product of DHFR activity, is used to synthesize 5,10-methylene-THF, which is eventually consumed in synthesis of methionine (through MetF/MetH), dTMP (through ThyA), and IMP (through FolD/PurH) (Figure S7A). In the presence of methionine in the medium, higher amounts of 5,10-methylene-THF can be channeled towards synthesis of dTMP and IMP. Second, both de novo purine and pyrimidine biosynthesis pathways require aspartate and glutamine (Figure S7B, C), which were otherwise low in minimal medium. Therefore, supplementation with amino acids removes this bottleneck, presumably leading to more efficient utilization of low THF amounts.

However, the question remains: Why are cells filamented despite rescue of purine and pyrimidine levels? Interestingly, we found that though dTMP levels much improved (to ~40-50% of WT levels) in the presence of amino acids, dTTP (thymidine derivative that is incorporated in the DNA) continued to be low, being only 3% of WT levels for I91L+W133V (at 40°C), and 18% for W133V (at 40°C) (Figure 3B for I91L+W133V; see Figure S5A, B for others; Figure S6 for metabolites as a function of time). In contrast, dATP and dCTP levels were very high (Figure 3B, Figure S5A, B). We hypothesize that misbalance in the concentrations of deoxy-nucleotides may lead to erroneous DNA replication, induction of SOS response and blocked cell division. Indeed, in our previous study, proteomics and transcriptomics analyses showed that several SOS response genes were upregulated in I91L+W133V and V75H+I91L+I155A strains at 37°C (Bershtein et al., 2015).

Filamentation and SOS response: Deletion of recA rescues filamentation

To gain a deeper understanding of the SOS response on growth medium conditions and filamentation, we quantified the expression of several SOS genes *recA*, *recN* and *sulA* under different supplementation conditions for mutant DHFR strains as well as TMP-treated WT cells. At 37°C, WT and mutant W133V were not elongated, and not surprisingly, they did not elicit any SOS response (Figure 4A-C). In comparison, I91L+W133V mutant (which is already elongated at 37°C) induced a strong SOS response with a 5-fold increase in *recA* expression, 7-fold increase in *recN* levels while *sulA* expression levels were 12-fold over WT (Figure 4A-C). At 42°C, where both W133V and I91L+W133V are elongated, all three genes had elevated expression compared to WT,

with expressions for I91L+W133V higher than those at 37°C (Figure S8). There was no induction of SOS response when cells were grown in the absence of amino acids, and much reduced levels of induction in the presence of thymine (dTMP), consistent with lack of filamentation under these two conditions (Figure 4A-C). Similar trends were also observed for WT treated with TMP.

RecA is the primary indicator of DNA damage, which cleaves the dimeric LexA repressor to turn on the genes that are under the SOS box (e.g., sulA, uvr proteins, *etc.*). SulA inhibits the cell division protein FtsZ, eventually causing filamentation. To understand the role of *recA* and *sulA* in our study, we treated *ΔrecA* and *ΔsulA* strains with near-MIC levels of the antibiotic TMP. As expected, *ΔrecA* strain did not show filamentation upon TMP treatment (Figure 4D), clearly highlighting its definitive role in filamentation. However, *ΔsulA* strain continued to filament (Figure 4D), indicating that *sulA*-independent pathways are also at play (Hill et al., 1997). Overall, these results clearly establish the role of the SOS pathway towards filamentation in mutant DHFR strains, which in turn is due to imbalance between dTTP and other deoxynucleotides in the cell.

Misbalance of deoxynucleotides is due to inhibition of Thymidylate Kinase (Tmk)

We next asked the question: why are dTTP levels low despite relatively high dTMP levels (Figure 5A)? The pyrimidine biosynthesis pathway (Figure S7C) involves conversion of dUMP to dTMP through Thymidylate synthase (ThyA). dTMP is then converted to dTDP using another essential enzyme Thymidylate Kinase (Tmk), which is further phosphorylated to form the triphosphate (dTTP) by Nucleotide Kinase (Ndk). To find out which step is getting inhibited, we looked at the levels of dTDP in mutant cells under conditions of filamentation. We found that dTDP levels were already low (Figure 5A), indicating that presumably the first step in the phosphorylation pathway involving Tmk is inhibited. Previous reports suggest that dUMP and dCTP can act as competitive inhibitors for Tmk (Nelson and Carter, 1969), and interestingly, we found that both dUMP and dCTP levels were highly upregulated in mutant cells (Figure S9), due to inefficient conversion of dUMP to dTMP in the presence of low DHFR activity (Figure S7C). We hypothesized that there might be two ways to overcome the competitive inhibition: a) to express more Tmk enzyme from a plasmid and b) to provide more of Tmk's natural substrate thymidylate monophosphate (dTMP) in the medium. To that end, we first measured cell length of mutant DHFR strains that were transformed with pBAD plasmid expressing Thymidylate Kinase (Tmk) from an arabinose inducible promoter. However, this experiment was inconclusive as expression of Tmk in WT strain

resulted in filamentation (Figure S10). Hence, we resorted to the second way to relieve inhibition: we grew WT and mutant strains in minimal medium that was supplemented with both amino acids and dTMP and carried out measurement of cell length as well as metabolomics as a function of time. We found that I91L+W133V mutant had much higher levels of both dTDP and dTTP relative to WT under this condition (Figure 5B). Since the ratio of product to substrate concentration should ideally reflect on the efficiency of an enzyme, we reasoned that this ratio should be higher for Tmk upon dTMP supplementation. Indeed, the ratio of dTDP:dTMP returned to WT levels for mutant I91L+W133V upon addition of dTMP in the medium (Figure 5C, upper panel), which was otherwise much below WT, indicating a relief of Tmk inhibition. In contrast, dTTP:dTDP ratios in both WT and mutant were similar even upon supplementation of dTMP (Figure 5C, lower panel), indicating that Ndk was not responsible for lowered dTTP levels in mutants. More importantly, addition of dTMP concomitantly rescued filamentation (Figure 5D). Since dATP/dCTP levels remained high despite addition of dTMP (Figure S11A), we conclude that higher amounts of dTTP presumably reduce the imbalance in relative concentrations of deoxy-nucleotides, thus relieving DNA damage and filamentation (see above)).

Moreover, supplementation of dTMP and amino acids also allowed mutants W133V, I91L+W133V and V75H+I91L+I155A to form higher counts of colony forming units (cfu) than with only amino acids at their respective filamentation temperatures (42°C for W133V and 40°C for I91L+W133V and V75H+I91L+I155A) (Figure 5E shows images for V75H+I91L+I155A). However, we note that cfu count for mutants in the presence of dTMP were still orders of magnitude lower than those of WT, indicating that thymine only rescues cell length, and not growth defects. This was also supported by the absence of growth rate rescue with dTMP (Figure S11B). However, when both purine source (GMP) and dTMP were supplemented along with amino acids, both cell length and growth rate were rescued (Figure 5D, S11B).

Filamentation in mutant DHFR strains is not due to TLD and is reversible

A moderate level of thymine deficiency – thymine limitation – affects cell shape by increasing its diameter but not the length, making cells less rod-like, and certainly not filamentous (Pritchard and Zaritsky, 1970; Zaritsky and Pritchard, 1973). A more severe level of thymine deprivation causes, under certain conditions, thymineless death (TLD), a phenomenon accompanied by cell filamentation (Ahmad et al., 1998; Bazill, 1967; Sangurdekar et al., 2011; Zaritsky et al., 2006).

Sangurdekar et al (Sangurdekar et al., 2010; Sangurdekar et al., 2011) also showed that thymine limitation is metabolically different from thymineless death, as DNA damage and SOS induction happens only in the latter, and cell death happening due to erroneous DNA replication. The phenotypic, metabolic as well as expression signatures of mutant DHFR strains seemed therefore, to resemble a case of thymine deprivation and TLD. To find out if mutant strains indeed represented a case of TLD, we assessed the viability of mutant strains at 30°C (permissive temperature) on solid media after several hours of growth at 42°C (restrictive temperature) in the presence of amino acids (filamentation condition). Sangurdekar et al (Sangurdekar et al., 2010) reported exponential loss in viability in TLD after one hour of growth under thymineless conditions. The idea was that if cells underwent TLD under conditions of filamentation, they would no longer be able to grow/form colonies at permissive temperature. We carried out this experiment in two different ways: First, we induced filamentous phenotype by incubating W133V mutant cells for 4 hours at 42°C, and then monitored cell recovery at room temperature (see *Materials and Methods*). Figure 6A shows a representative example of morphology of W133V filament that begins to undergo slow division initiated at the poles at permissive temperature. Most progeny cells of normal size appeared after 5-6 hours of growth at low temperature. Second, we grew mutant strains at 42°C for 6 hours, and subsequently allowed them to grow at 30°C (permissive temperature) on solid media to check colony forming ability (Figure 6B). Surprisingly, both W133V and I91L+W133V mutants grew to similar extents as WT at the permissive temperature after 6 hours of growth at restrictive temperature, indicating no loss in viability (Figure 6B). Both these experiments clearly demonstrated that despite the extensive DNA damage and filamentation, mutant cells did not represent a case of TLD. Interestingly, even when WT cells were treated with varying concentrations of TMP at 42°C in the presence of amino acids, there was no loss in viability at any concentration tested (Figure 6C). Rather, cfu counts did not change at concentrations higher than MIC, indicating that in minimal media supplemented with amino acids, TMP as well as mutants are bacteriostatic and not bactericidal.

Mutants do not cause TLD even upon purine supplementation

Kwon *et al* (Kwon et al., 2010) showed that when both amino acid and a purine source are supplemented, lethal doses of TMP treatment leads to TLD. To test the validity of this result at lower concentrations of TMP, we treated WT *E. coli* cells with a gradient of TMP concentrations

for 6 hours at 42°C in the presence of both amino acids and a purine source (GMP) and assayed for viability at permissive temperature following that. As shown in Figure 7A, cells showed loss in viability only at TMP concentrations near to or higher than the MIC (≥1μg/ml). Since mutant cells mimic sublethal concentrations of TMP treatment (~0.5μg/ml), we hypothesized that even mutants should retain viability after exposure to amino acid and GMP at high temperature. Indeed, cells retained viability as good as without added purine source (Figure 6B), indicating again that filamentation is completely reversible. In terms of phenotype, mutant cells grown with amino acids and GMP were not only filamentous, but also exhibited condensed nucleoids, presumably indicating severity of DNA damage (Figure 7B, C). As expected, metabolomics under this condition showed extreme imbalance in relative levels of deoxynucleotides: extremely high dATP and dCTP levels, while dTTP levels were too low to detect (Figure 7D). Not surprisingly, addition of a purine source largely increased the extent of DNA damage as shown by the SOS response genes (Figure 7E). Despite this, the fact that cells were still viable shows that to a large extent, DNA damage can be recovered. This is also exemplified from our previous study which showed significant upregulation of DNA damage repair genes in filamentous strains, besides SOS genes (Bershtein et al., 2015). Nevertheless, this study highlights the considerable overlap that exists between characteristics of thymine limitation and thymineless death and emphasizes the fact that these two conditions are not an all or none phenomenon.

Discussion

Metabolic networks of cells are inherently intertwined, with substrates and products of one pathway being utilized by another pathway. As a result, perturbations produced in one pathway can easily percolate into others, usually magnifying effects. The folate pathway or the 1-carbon metabolism pathway is a classic example of this, as reduced folates act as 1-carbon donors during biosynthesis of purines, pyrimidines and amino acids. Kwon et al (Kwon et al., 2008) showed that for inhibition of DHFR activity using trimethoprim, accumulation of substrate dihydrofolate (DHF), in turn, results in inhibition of another downstream enzyme critical to folate metabolism: folylpoly-gamma-glutamate synthetase (FP-gamma-GS), much like a domino effect (falling DHFR activity triggers a fall in the other enzyme's activity too). A similar domino effect was also observed for the drug Phloretin in *Trypanosoma brucei*, which functions primarily by inhibiting the glucose transporter of the deadly parasite. However, the drug also causes down-regulation of the

transporter mRNA levels as well as drop in the glycolytic flux, thus rendering the parasite even more vulnerable to the drug (Haanstra et al., 2011).

In this work, we show that in *E. coli* strains that harbor destabilizing mutations in *folA* gene, reduced DHFR activity is reflected, among other factors, in the pyrimidine biosynthesis pathway by inefficient production of dTMP from dUMP via thymidylate synthase (ThyA) that uses a derivative of THF as one carbon source. This causes accumulation of upstream metabolites dUMP and dCTP, which happen to be competitive inhibitors of the next enzyme in the pathway Thymidylate Kinase (Tmk). As a result, phosphorylation of dTMP to dTDP and eventually dTTP is inhibited. Drop in dTTP and accumulation of dCTP/dATP leads to an imbalance in the levels of deoxynucleotides, eventually causing errors in DNA replication, SOS response and filamentation. This study, therefore, presents an instance of a domino effect in the *E. coli* folate and pyrimidine biosynthesis pathway. Surprisingly, this is not largely manifested in minimal medium, where severe depletion of methionine levels stalls growth. Only when purine (IMP) and pyrimidine (dTMP) levels get partially rescued due to amino acid supplementation and the cell attempts to grow, inhibition of Tmk and subsequent drop in dTTP (despite moderate availability of dTMP) causes cells to filament.

In our case, mutant DHFR strains accumulate very high levels of dUMP and dCTP, hence we presume that Tmk inhibition arises through competitive binding of dUMP at the dTMP binding site and of dCTP at the ATP binding site (Nelson and Carter, 1969). Such instances where structural homologs of substrates act as competitive inhibitors are relatively common in nucleotide binding enzymes. It has been shown that binding of GTP at the ATP binding site can inhibit the activity of adenylate kinase (Rogne et al., 2018), while nucleotide kinase (Ndk) can use a relatively diverse set of nucleotide triphosphates and diphosphates as phosphate donors and acceptors, respectively (Roisin and Kepes, 1978). However, enzymes overcome this apparent lack of substrate selectivity by maintaining fine balance among metabolite concentrations inside the cell. For example, undetectably low levels of dUMP in WT cells prevent inhibition of Tmk under normal conditions. Intracellular dCTP levels are generally much smaller than ATP (35μM dCTP vs 9.6mM of ATP) (Bennett et al., 2008). However, mutant DHFR cells accumulate dCTP more than 14 times over WT levels while ATP increases by 3 fold, thereby increasing the overall likelihood of inhibition. Therefore, under conditions of loss of metabolic homeostasis in the cell, several enzymes that utilize nucleotide (mono-, di-, tri-) phosphates as substrates become especially

vulnerable to inhibition of function through promiscuous binding of ligands that are structural mimics. Hence, our case of Tmk inhibition might be more of a norm rather than an exception.

A remarkable aspect of the current study is the finding is that mutant DHFR cells do not lose viability despite indications of substantial DNA damage. This points to the large buffering capacity of the cell in terms of repair of damaged DNA. This is also supported by our earlier finding based on proteomics and transcriptomics data that besides SOS pathway proteins, DNA damage repair proteins were also significantly upregulated (Bershtein et al., 2015). Sangurdekar *et al* (Sangurdekar et al., 2010; Sangurdekar et al., 2011) argue that DNA damage is the most salient feature that distinguishes between thymine limitation and thymineless death (TLD). Our results however indicate that it is possible to incur DNA damage and still retain reversibility. In fact, our data indicates that thymine limitation and TLD are the two ends of a spectrum, with considerable variability in between.

Several previous studies (Amyes and Smith, 1974; Kwon et al., 2010; Sangurdekar et al., 2011) have showed that high concentrations of antibiotic trimethoprim (5-6μg/ml) induce thymineless death in rich medium. Here, by systematically varying the concentration of TMP, we show that TMP is only bacteriostatic at or below the MIC, even in rich media supplemented with both amino acids and purines, and TLD happens only at lethal doses of the drug. Conversely, in minimal medium supplemented only with amino acids, near-MIC level of the drug causes filamentation like mutant DHFR strains. Overall, reversible filamentation and DNA damage under this condition might play an important role in the evolution of antibiotic resistance and persistence at sub-lethal TMP concentrations.

Unlike eukaryotic cells which have distinct stages of cell cycle and growth, prokaryotes like *E. coli* coordinate cytoplasmic growth, DNA replication and cell division simultaneously to achieve balanced growth. It has been argued that it is cellular metabolism that efficiently coordinates these processes (Sperber and Herman, 2017). Several metabolic pathways, for example TCA cycle (Monahan et al., 2014), nitrogen metabolism (Beaufay et al., 2015), pyruvate metabolism (Monahan et al., 2014), glucose metabolism (Hill et al., 2013; Weart et al., 2007), etc., have been implicated to control cell shape and size. One or more proteins in these pathways have moonlighting functions, whereby they directly interact with the main modulators of cell division, MreB and FtsZ besides carrying out their own enzymatic function. In this work, mutant DHFRs modulate cell length through the SOS pathway, which ultimately blocks division through a SulA

dependent or independent pathway. This is unlike most other pathways, where the mechanism is through direct interaction with MreB or FtsZ. Regardless of the mechanism, this work uncovers how another central metabolic pathway, the folate or 1-carbon metabolism pathway can reversibly modulate size and shape of *E. coli* in a mechanism that is fundamentally different from TLD.

Acknowledgements

This work was supported by NIH grant GM068670 to E.I.S.

Author contributions

Conceptualization, S.Bh., S.Be., and E.I.S.; Methodology, S.Bh., S.Be., B.V.A., J.W., and E.I.S.; Formal Analysis, S.Bh., S.Be., and E.I.S.; Investigation, S.Bh., S.Be, B.V.A., J.W.; Writing-original draft, S.Bh., and E.I.S.; writing-review & editing, S.Bh., S.Be., B.V.A., and E.I.S.; Supervision, E.I.S.; Funding acquisition, E.I.S.

Figure legends

Figure 1: Destabilizing mutations in DHFR induce filamentous phenotype. (A) Growth rates of mutant DHFR strains at 30°C, 37°C and 42°C. While most mutants grow well at 30°C, they grow very poorly at high temperatures. Error bars represent SEM of three biological replicates. (B) Distribution of cell lengths of WT and mutants W133V and V75H+I155A at 42°C (gray box) and I91L+W133V at 40°C (represented as white box) after being grown in M9 minimal medium for 4 hours. Median cell length of W133V and V75H+I155A is significantly smaller than WT (Mann-Whitney test, p-value <0.001). Live cells DIC images and DAPI nucleoids staining of (C) WT DHFR and (D) I91L+W133V DHFR strains after being grown at 30°C, 37°C, or 42°C (I91L+W133V was grown at 40°C) in M9 medium supplemented with amino acids for 4 hours (see *Materials and Methods*). Cell lengths were measured from the obtained DIC images (see *Materials and Methods*) and their distribution at 37°C and 40°C/42°C is shown in (E) and (F) as box-plots. Images of other mutant DHFR strains W133V, V75H+I155A and V75H+I91L+I155A are presented in related Figure S1.

Figure 2: Filamentation in mutant DHFR strains is due to loss of DHFR activity. WT and mutant DHFR strains were transformed with pBAD plasmid that expressed WT DHFR under control of arabinose promoter. Transformed cells were grown at 42°C (for WT, W133V and V75H+I155A strains) or at 40°C (for I91L+W133V and V75H+I91L+I155A) in M9 medium supplemented with amino acids. Functional complementation of WT DHFR rescues both (A) filamentation and (B) growth defects of mutant strains. Expression of mutant proteins from pBAD plasmid on the WT background does not result in (C) filamentation or (D) growth defects. (E) Treatment of WT *E. coli* cells at 42°C with the antifolate drug Trimethoprim (TMP) in amino acid supplemented M9 medium results in filamentation, with the maximum elongation happening below or near MIC of the drug (1μg/ml). See related Figure S4 for distribution of cell length as a function of TMP concentration at 37°C, where the effect is less prominent. (F) Addition of TMP to filamented mutant V75H+I155A at 42°C results in gradual reduction in filamentation, possibly due to growth arrest. See related figures S3 and S4.

Figure 3: Metabolomics of mutant DHFR strains in minimal media without or with added amino acids. (A) and (C) shows abundance of selected nucleotides and amino acids for mutant

I91L+W133V after 4 hours of growth at 40°C in M9 minimal medium (no filamentation), while (B) and (D) represents nucleotide and amino acid abundances after 4 hours of growth in amino acid supplemented M9 medium at 40°C (condition of filamentation). Concentration of all metabolites were normalized to WT levels at 4 hours when grown under similar conditions. In minimal medium (C), Methionine levels are extremely low, which recover in panel (D). Levels of purines (IMP, AMP) as well as pyrimidines (dTMP) are rescued with amino acid supplementation, however dTDP and dTTP levels remain extremely low. Error bars represent SD of 2-3 biological replicates (see *Methods*). See related figures S5A-B, S6, Table S1.

Figure 4: Filamentation in mutant DHFR strains is associated with strong SOS response. Expression of (A) *recA* (B) *recN* and (C) *sulA* genes measured by quantitative PCR when WT and mutant strains are grown in M9 medium with or without supplementation of amino acids or dTMP. WT and mutant strains were grown for 4 hours of growth in the indicated medium at 37°C, while WT treated with different concentrations of TMP were grown for 4 hours at 42°C. Brown bars (M9+AA) in the gray shaded area correspond to filamentation conditions and these are associated with pronounced upregulation of all three SOS genes. On the other hand, conditions with loss of filamentation (with dTMP or no supplementation) show much less expression. Error bars represent SD of 2-3 biological replicates (see *Methods*). (D) Treatment of WT *E. coli* cells with sub-MIC concentration of TMP (0.5μg/ml) leads to filamentation at 42°C when grown in amino acid supplemented medium. However, a *recA* knock-out strain under similar condition shows no elongation, indicating the role of SOS pathway in filamentation. A *sulA* knock-out continues to elongate, indicating the role of *sulA*-independent pathways. See related Figure S8.

Figure 5: Filamentation is due to Tmk inhibition and low levels of dTTP. (A) Levels of different thymidine nucleotides dTMP, dTDP and dTTP in WT, W133V and I91L+W133V mutants as a function of time when grown in M9 medium supplemented with amino acids (M9+AA) at 42°C (40°C for I91L+W133V). All metabolites levels were normalized to WT levels at 2 hours (set to 1). Though dTMP levels in mutants is ~50% of WT, dTDP and dTTP levels are severely depleted. (B) Abundances of thymidine nucleotides dTMP, dTDP and dTTP in WT and I91L+W133V mutant as a function of time when grown in M9 medium supplemented with amino acids and 1mM dTMP (M9+AA+dTMP) at 42°C (40°C for I91L+W133V). All

metabolites levels were normalized to WT levels at 2 hours (set to 1). Error bars represent SD of 2-3 biological replicates. (C) Ratios of dTDP/dTMP levels (upper panel) and dTTP/dTDP levels (lower panel) for WT (grey) and I91L+W133V mutant (yellow) as a function of time when grown in either M9 medium supplemented with amino acids (light colored bars) or in M9 medium supplemented with amino acids and 1mM dTMP (dark colored bars). dTDP/dTMP levels which reflect on the efficiency of Tmk improve substantially for I91L+W133V mutant and reach to WT levels upon dTMP supplementation. On the other hand, dTTP/dTDP levels which reflect on efficiency of Ndk does not change in the presence of dTMP. For I91L+W133V mutant in amino acid supplemented medium (light yellow bars), dTTP levels dropped below detectable limits at 6 and 8 hours, hence dTTP/dTDP ratios at these time points could not be computed (N.D.). (D) Distribution of cell length of WT and mutant strains when grown in M9 medium supplemented with amino acids (gray) or with both amino acids and 1mM dTMP (pink) or with folate mix (blue). WT, W133V and V75H+I155A strains were grown at 42°C while I91L+W133V and V75H+I91L+I155A mutants were grown at 40°C. 1mM dTMP largely rescues filamentation of mutant strains, while metabolic complementation of DHFR activity with folate mix (see *Methods*) completely brings it to WT levels (* indicates the distribution of cell lengths were significantly different, Mann-Whitney test, p-value <0.001) (E) Mutant V75H+ I91L+I155A grows very poorly (in terms of colony forming units, cfu) on a minimal media agar plate supplemented with amino acids (M9+AA) at 40°C. Supplementation of additional dTMP increases the cfu by several orders at the same temperature, while supplementation with both dTMP and purine (GMP) allows it to grow as good as WT. In comparison, WT was grown at 42°C under different supplementation conditions. In all cases, cultures were 7-fold serially diluted for the next spot. The three rows (two rows for WT) in each condition represent biological replicates. See related figures S7, S9, S10 and S11.

Figure 6: Filamentation in mutant DHFR strains is completely reversible. (A) Mutant W133V was grown in amino acid supplemented M9 medium for 4 hours at 42°C, and subsequently placed on M9 agar pads and their growth was monitored at room temperature. Shown are phase contrast images taken from different time points throughout the time-lapse experiment. Unlike cells experiencing TLD, an irreversible phenomenon, W133V DHFR cells recover and resume growth at low temperature. (B) WT and mutants were grown as in (A) for 6 hours at 42°C and subsequently diluted serially and spotted on amino acid supplemented M9

agar plates and allowed to grow at 30°C till visible colonies were formed. (C) WT cells were treated with different concentrations of TMP at 42°C for varying amounts of time, following which they were spotted on amino acid supplemented M9 plates and allowed to grow at 30°C. There was no loss in viability for any concentration of TMP, thus showing in amino acid supplemented medium TMP is only bacteriostatic despite extensive filamentation. Error bars represent SD of three biological replicates.

Figure 7: Effect of purine source supplementation on mutant and TMP treated WT cells. (A) WT cells were treated with different concentrations of TMP at 42°C in M9 media supplemented with both amino acids and purine (GMP) for varying amounts of time, following which they were spotted on amino acid supplemented M9 plates and allowed to grow at 30°C. The cells showed sharp loss in viability when grown at TMP concentrations equal to greater than the MIC (1μg/ml). This contrasts with Figure 6C, where no loss in viability was observed. Error bars represent SD of three biological replicates. (B) Live cells DIC images of I91L+W133V DHFR cells grown for 4 hours at 40°C in M9 medium supplemented with amino acids (C) Addition of 2mM GMP to (B) resulted in elongated morphology and condensed single nucleoids (DAPI staining, cyan). (D) Metabolomics of I91L+W133V strain at 42°C in M9 medium supplemented with both amino acids and purine (GMP) shows severe imbalance among concentrations of deoxynucleotides (~1000 fold upregulation of dATP, dCTP, while dTTP levels were undetectably low). Error bars represent SD of 2-3 biological replicates. Expression of SOS response genes (E) *recA* (F) *recN* and (G) *sulA* when mutant strains and TMP treated WT cells are grown in M9 medium supplemented with amino acids (black bars) or in the presence of both amino acids and GMP (gray bars) at 42°C (I91L+W133V was grown at 40°C). Though TLD only happens at TMP concentrations ≥1μg/ml in the presence both amino acids and GMP, expression of SOS genes in unable differentiate between the bacteriostatic and bactericidal regimes. Error bars represent SD of 2-3 biological replicates.

STAR Methods

Strains and media. The design principles of mutant DHFR strains were reported previously (Bershtein et al, 2012). M9 minimal medium *without amino acids* was only supplemented with 0.2% glucose and 1mM $MgSO_4$ while M9 media *with amino acids* was supplemented with 0.2% glucose, 1mM $MgSO_4$, 0.1% casamino acids, and 0.5 μg/ml thiamine. Casamino acids is a commercially available mixture of all amino acids except tryptophan, and cysteine is present in a very small amount. Wherever mentioned, 1mM GMP was used as a source of purine, while 1mM dTMP (thymidine monophosphate) was used as a source of thymine. Folate mix consists of M9 minimal medium supplemented with 1 mM adenine, 1 mM thymine, 1 μg/mL D-panthothenate, 0.5 mM glycine, and 0.5 mM methionine.

Growth conditions. All strains were grown overnight from a single colony at 30°C, and subsequently the culture was diluted to a final OD_{600} of 0.01 in the specified medium and allowed to grow for 16-18 hours in Bioscreen C (Growth Curves, USA) at 30°C, 37°C or 42°C. Growth curves were fit to a 4-parameter Gompertz equation as described in (Bhattacharyya et al., 2017) to derive growth parameters. Error bars were calculated as SEM of three biological replicates.

Light microscopy. Cells were grown overnight at 30°C from a single colony in the specified medium, diluted 1/100, and grown at various temperatures for 4 hours. For DIC images in Figures 1C, 1D, 7B, 7C and Figure S1, cells were pelleted, washed with PBS, and concentrated. DAPI staining (Molecular probes) was performed for 10 min at RT according to manufacturer instructions. 1 μl of a concentrated culture was then mounted on a slide and slightly pressed by a cover slip. DIC and DAPI images were obtained at room temperature by Nikon Ti Eclipse Microscope equipped with iXon EMCCD camera (Andor Technologies). For live phase contrast images and time-lapse experiments (Figure 6A), cells were mounted on supplemented M9 + 1.5% low melting agarose (Calbiochem) pads. Pads were then flipped on #1.5 glass dish (Willco Wells), and the images were acquired at room temperature with Zeiss Cell Observer microscope. For DIC images in Figure S9, cells were placed on agar pads and images were acquired with Zeiss Cell Discoverer microscope.

Analysis of cell lengths. MicrobeTracker Suite [http://microbetracker.org/](Sliusarenko et al., 2011) was used to obtain distributions of cell length for phase contrast images and Zeiss

Intellesis Module was used to analyze DIC images. On average, 500 cells were analyzed for each presented distribution.

Statistical analysis. In our experiments, cell lengths of *E. coli* were not normally distributed. Hence non-parametric Mann-Whitney test was used to determine if the distribution of cell lengths of two samples were significantly different.

Metabolomics. Cells were grown overnight at 30°C from a single colony in the specified medium, diluted 1/100, and re-grown. WT, WT+0.5μg/ml TMP and W133V mutant were grown at 42°C, while mutant I91L+W133V was grown at 40°C. For time course experiment, aliquots were removed after 2, 4, 6 and 8 hours, and metabolites were extracted as described in (Bhattacharyya et al., 2016). Metabolite levels were averaged over 2-3 biological replicates. A linear regression of replicate SD vs the replicate average showed that absolute errors (constant) was nearly zero, while relative errors were ~15% of the mean. Hence error bars in Figures 3, 4(A, B), 7D, Figure S5, S8, S10A represent 15% of the mean value.

Expression of SOS response genes by qPCR. Cells were grown overnight at 30°C from a single colony in the specified medium, diluted 1/100, and grown at 37°C or 42°C for 4 hours. Based on OD_{600} of the cultures, a volume equivalent to 5×10^8 cells were spun down (assuming 1 $OD_{600}=8\times10^8$ cells) and Protect Bacteria RNA Mini Kit (Qiagen) was used to extract total RNA as described in (Bhattacharyya et al., 2018). Following reverse transcription (Bhattacharyya et al., 2018), expression of *recA*, *recN* and *sulA* genes were quantified using QuantiTect SYBR Green PCR kit (Qiagen) using the following primers:

recA_fwd	ACAAACAGAAAGCGTTGGCG
recA_rev	AGCGCGATATCCAGTGAAAG
recN_fwd	TTGGCACAACTGACCATCAG
recN_rev	GACCACCGAGACAAAGAC
sulA_fwd	GTACACTTCAGGCTATGCAC
sulA_rev	GCAACAGTAGAAGTTGCGTC

As it was difficult to find a reference gene that would be expressed to similar levels in WT vs mutant DHFR strains, we used total RNA to normalize the expression levels.

Expression levels reported are average of 2-3 biological replicates. A similar error analysis as discussed in Metabolomics section showed that relative errors were ~12% of the mean. Hence error bars in Figures 4(A, B, C) and 7(E, F, G) represent 12% of the mean value.

Supplemental Information

The manuscript contains 11 Supplementary figures (Figure S1-S11) and 1 Supplementary table.

Table S1: Comprehensive metabolomics data

Supplementary Figure Captions

Figure S1. Destabilizing mutations in DHFR induce filamentous phenotype. Live cells DIC images with DAPI nucleoids staining of W133V, V75H+I155A, and V75H+I91L+I155A DHFR E. coli MG1655 strains. Prior to microscopy, cells were grown at 30°C, 37°C, and 42°C (V75H+I91L+I155A was grown at 40°C) in amino acid supplemented M9 medium for 4 hours (see Materials and Methods).

Figure S2. Intracellular abundance of WT and mutant DHFRs measured by Western blot. WT, W133V and V75H+I155A were grown for 4 hours at 42°C while I91L+W133V and V75H+I91L+I155A strains were grown for 4 hours at 40°C in amino acid supplemented M9 medium before being harvested. The data is also reported in (Bershtein et al., 2015).

Figure S3. The effect of WT DHFR inhibition by trimethoprim (TMP) on growth. WT DHFR cells were grown at 42°C in amino acid M9 medium, and their growth was monitored by OD at 600nm. The data were fit to a 4-parameter Gompertz equation as described in (Bhattacharyya et al., 2017) to derive growth parameters.

Figure S4. Distribution of cell length of WT E. coli as a function of TMP concentration when grown in amino acid supplemented M9 medium at 37°C. Concentrations of TMP near the MIC results in maximum filamentation, while the effect dies down at higher concentrations. Filamentation is much pronounced when cells are grown at 42°C (see Figure 2E).

Figure S5. Metabolomics of (A) W133V DHFR strain and (B) WT treated with 0.5μg/ml Trimethoprim in minimal media at 42°C with or without added amino acids. The bars represent abundance of selected nucleotides and amino acids after 4 hours of growth in the indicated medium. Concentration of all metabolites were normalized to WT levels when grown under similar conditions. Error bars represent SD of 2-3 biological replicates. For both (A) and (B), methionine levels were extremely low in the absence of amino acids, which rise substantially when grown in the presence of amino acids. Though purines and pyrimidines also improve with amino acid supplementation, dTDP and dTTP levels remain poor.

Figure S6. Abundances of metabolites IMP, ATP, dTMP and dTTP levels as a function of time for WT *E. coli* without and with 0.5µg/ml TMP as well as mutants W133V and I91L+W133V when grown in amino acid supplemented M9 medium at 42°C (40°C for I91L+W133V). The plot also includes metabolite abundances for WT and I91L+W133V grown in the presence of 1mM dTMP in amino acid supplemented M9 medium. All values are normalized with respect to abundance of that metabolite obtained for WT after 2 hours of growth.

Figure S7. Schematic representation of (A) 1-carbon metabolism metabolism pathway (adapted from (Bhattacharyya et al., 2016)) (B) *de novo* purine biosynthesis pathway and (C) *de novo* pyrimidine biosynthesis pathway.

Figure S8. Comparison of expression of SOS response genes (A) *recA* (B) *recN* and (C) *sulA* measured by quantitative PCR for WT and mutant strains grown at 37°C vs at 42°C in amino acid supplemented M9 medium. More pronounced filamentation at higher temperature is associated with greater induction of SOS response genes. Error bars represent SD of 2-3 biological replicates.

Figure S9. Abundances of metabolites (A) dCTP and (B) dUMP as a function of time for WT, W133V and I91L+W133V mutants when grown in amino acid supplemented M9 medium at 42°C (40°C for I91L+W133V). dCTP levels were normalized to those obtained for WT after 2 hours of growth. dUMP levels were undetectable in WT, hence the absolute intensities per milligram of dry weight of *E. coli* as detected by mass spectrometry is shown in (B). Error bars represent SD of 2-3 biological replicates.

Figure S10. DIC image of untransformed WT *E. coli* cells as well as WT transformed with pBAD plasmid that expresses Thymidylate Kinase under control of arabinose promoter. Cells were grown at 42°C for 4 hours in amino acid supplemented M9 medium in the presence of 0.2% of arabinose. Expression of Tmk in WT cells results in filamentation.

Figure S11. (A) Abundances of selected nucleotides in I91L+W133V mutant when grown for 4 hours at 40°C in M9 medium supplemented with both amino acids and 1mM dTMP. Metabolite levels were normalized to those of WT grown under similar conditions. dTDP and dTTP levels recover and are now comparable to dTMP levels due to relief of competitive inhibition of Thymidylate Kinase. Error bars represent SD of 2-3 biological replicates. (B) Comparison of growth rates of WT and mutant DHFR strains at 42°C (40°C for I91L+W133V and V75H+I91L+I155A) in minimal medium that is supplemented with amino acids and/or

1mM dTMP or in the presence of folate mix (see *Materials and Methods*). Except for W133V and to a lesser extent for V75H+I155A, the effect of dTMP on growth rates is only modest. Folate mix however brings back growth rates close to WT levels, even for the poorest mutants I91L+W133V and V75H+I91L+I155A. Error bars represent SEM of 3 biological replicates.

References

Addinall, S.G., Small, E., Whitaker, D., Sturrock, S., Donachie, W.D., and Khattar, M.M. (2005). New temperature-sensitive alleles of ftsZ in Escherichia coli. J Bacteriol *187*, 358-365.

Ahmad, S.I., Kirk, S.H., and Eisenstark, A. (1998). Thymine metabolism and thymineless death in prokaryotes and eukaryotes. Annu Rev Microbiol *52*, 591-625.

Amyes, S.G., and Smith, J.T. (1974). Trimethoprim action and its analogy with thymine starvation. Antimicrob Agents Chemother *5*, 169-178.

Bazill, G.W. (1967). Lethal unbalanced growth in bacteria. Nature *216*, 346-349.

Beaufay, F., Coppine, J., Mayard, A., Laloux, G., De Bolle, X., and Hallez, R. (2015). A NAD-dependent glutamate dehydrogenase coordinates metabolism with cell division in Caulobacter crescentus. EMBO J *34*, 1786-1800.

Bennett, B.D., Yuan, J., Kimball, E.H., and Rabinowitz, J.D. (2008). Absolute quantitation of intracellular metabolite concentrations by an isotope ratio-based approach. Nat Protoc *3*, 1299-1311.

Bershtein, S., Choi, J.M., Bhattacharyya, S., Budnik, B., and Shakhnovich, E. (2015). Systems-level response to point mutations in a core metabolic enzyme modulates genotype-phenotype relationship. Cell reports *11*, 645-656.

Bershtein, S., Mu, W., Serohijos, A.W., Zhou, J., and Shakhnovich, E.I. (2013). Protein Quality Control Acts on Folding Intermediates to Shape the Effects of Mutations on Organismal Fitness. Molecular cell *49*, 133-144.

Bershtein, S., Mu, W., and Shakhnovich, E.I. (2012). Soluble oligomerization provides a beneficial fitness effect on destabilizing mutations. Proc Natl Acad Sci U S A *109*, 4857-4862.

Bhattacharyya, S., Bershtein, S., and Shakhnovich, E.I. (2017). Gene Dosage Experiments in Enterobacteriaceae Using Arabinose-regulated Promoters. Bio-Protocol *7*, e2396.

Bhattacharyya, S., Bershtein, S., Yan, J., Argun, T., Gilson, A.I., Trauger, S.A., and Shakhnovich, E.I. (2016). Transient protein-protein interactions perturb E. coli metabolome and cause gene dosage toxicity. Elife *5*.

Bhattacharyya, S., Jacobs, W.M., Adkar, B.V., Yan, J., Zhang, W., and Shakhnovich, E.I. (2018). Accessibility of the Shine-Dalgarno Sequence Dictates N-Terminal Codon Bias in E. coli. Molecular cell *70*, 894-905 e895.

Bi, E., and Lutkenhaus, J. (1990). Analysis of ftsZ mutations that confer resistance to the cell division inhibitor SulA (SfiA). J Bacteriol *172*, 5602-5609.

Bollenbach, T., Quan, S., Chait, R., and Kishony, R. (2009). Nonoptimal microbial response to antibiotics underlies suppressive drug interactions. Cell *139*, 707-718.

Champion, J.A., and Mitragotri, S. (2006). Role of target geometry in phagocytosis. Proc Natl Acad Sci U S A *103*, 4930-4934.

Dai, X., Shen, Z., Wang, Y., and Zhu, M. (2018). Sinorhizobium meliloti, a Slow-Growing Bacterium, Exhibits Growth Rate Dependence of Cell Size under Nutrient Limitation. mSphere *3*.
Fonville, N.C., Bates, D., Hastings, P.J., Hanawalt, P.C., and Rosenberg, S.M. (2010). Role of RecA and the SOS response in thymineless death in Escherichia coli. PLoS genetics *6*, e1000865.
Haanstra, J.R., Kerkhoven, E.J., van Tuijl, A., Blits, M., Wurst, M., van Nuland, R., Albert, M.A., Michels, P.A., Bouwman, J., Clayton, C., *et al.* (2011). A domino effect in drug action: from metabolic assault towards parasite differentiation. Mol Microbiol *79*, 94-108.
Hill, N.S., Buske, P.J., Shi, Y., and Levin, P.A. (2013). A moonlighting enzyme links Escherichia coli cell size with central metabolism. PLoS genetics *9*, e1003663.
Hill, T.M., Sharma, B., Valjavec-Gratian, M., and Smith, J. (1997). sfi-independent filamentation in Escherichia coli Is lexA dependent and requires DNA damage for induction. J Bacteriol *179*, 1931-1939.
Hiraga, S., Niki, H., Ogura, T., Ichinose, C., Mori, H., Ezaki, B., and Jaffe, A. (1989). Chromosome partitioning in Escherichia coli: novel mutants producing anucleate cells. J Bacteriol *171*, 1496-1505.
Horvath, D.J., Jr., Li, B., Casper, T., Partida-Sanchez, S., Hunstad, D.A., Hultgren, S.J., and Justice, S.S. (2011). Morphological plasticity promotes resistance to phagocyte killing of uropathogenic Escherichia coli. Microbes Infect *13*, 426-437.
James, G.A., Korber, D.R., Caldwell, D.E., and Costerton, J.W. (1995). Digital image analysis of growth and starvation responses of a surface-colonizing Acinetobacter sp. J Bacteriol *177*, 907-915.
Justice, S.S., Hunstad, D.A., Seed, P.C., and Hultgren, S.J. (2006). Filamentation by Escherichia coli subverts innate defenses during urinary tract infection. Proc Natl Acad Sci U S A *103*, 19884-19889.
Kruse, T., Moller-Jensen, J., Lobner-Olesen, A., and Gerdes, K. (2003). Dysfunctional MreB inhibits chromosome segregation in Escherichia coli. Embo J *22*, 5283-5292.
Kwon, Y.K., Higgins, M.B., and Rabinowitz, J.D. (2010). Antifolate-induced depletion of intracellular glycine and purines inhibits thymineless death in E. coli. ACS Chem Biol *5*, 787-795.
Kwon, Y.K., Lu, W., Melamud, E., Khanam, N., Bognar, A., and Rabinowitz, J.D. (2008). A domino effect in antifolate drug action in Escherichia coli. Nature chemical biology *4*, 602-608.
Monahan, L.G., Hajduk, I.V., Blaber, S.P., Charles, I.G., and Harry, E.J. (2014). Coordinating bacterial cell division with nutrient availability: a role for glycolysis. MBio *5*, e00935-00914.
Monds, R.D., Lee, T.K., Colavin, A., Ursell, T., Quan, S., Cooper, T.F., and Huang, K.C. (2014). Systematic perturbation of cytoskeletal function reveals a linear scaling relationship between cell geometry and fitness. Cell reports *9*, 1528-1537.
Nelson, D.J., and Carter, C.E. (1969). Purification and characterization of Thymidine 5-monophosphate kinase from Escherichia coli B. J Biol Chem *244*, 5254-5262.
Ogura, T., Bouloc, P., Niki, H., D'Ari, R., Hiraga, S., and Jaffe, A. (1989). Penicillin-binding protein 2 is essential in wild-type Escherichia coli but not in lov or cya mutants. J Bacteriol *171*, 3025-3030.
Pernthaler, J. (2005). Predation on prokaryotes in the water column and its ecological implications. Nat Rev Microbiol *3*, 537-546.

Persat, A., Stone, H.A., and Gitai, Z. (2014). The curved shape of Caulobacter crescentus enhances surface colonization in flow. Nat Commun *5*, 3824.
Pichoff, S., Shen, B., Sullivan, B., and Lutkenhaus, J. (2012). FtsA mutants impaired for self-interaction bypass ZipA suggesting a model in which FtsA's self-interaction competes with its ability to recruit downstream division proteins. Mol Microbiol *83*, 151-167.
Pine, L., and Boone, C.J. (1967). Comparative cell wall analyses of morphological forms within the genus Actinomyces. J Bacteriol *94*, 875-883.
Pritchard, R.H., and Zaritsky, A. (1970). Effect of thymine concentration on the replication velocity of DNA in a thymineless mutant of Escherichia coli. Nature *226*, 126-131.
Rodrigues, J.V., Bershtein, S., Li, A., Lozovsky, E.R., Hartl, D.L., and Shakhnovich, E.I. (2016). Biophysical principles predict fitness landscapes of drug resistance. Proc Natl Acad Sci U S A.
Rodrigues, J.V., and Shakhnovich, E. (2019). Evolutionary dynamics determines adaptation to inactivation of an essential gene. bioRxiv.
Rogne, P., Rosselin, M., Grundstrom, C., Hedberg, C., Sauer, U.H., and Wolf-Watz, M. (2018). Molecular mechanism of ATP versus GTP selectivity of adenylate kinase. Proc Natl Acad Sci U S A *115*, 3012-3017.
Roisin, M.P., and Kepes, A. (1978). Nucleosidediphosphate kinase of Escherichia coli, a periplasmic enzyme. Biochimica et biophysica acta *526*, 418-428.
Ruoff, K.L. (1991). Nutritionally variant streptococci. Clin Microbiol Rev *4*, 184-190.
Sangurdekar, D.P., Hamann, B.L., Smirnov, D., Srienc, F., Hanawalt, P.C., and Khodursky, A.B. (2010). Thymineless death is associated with loss of essential genetic information from the replication origin. Mol Microbiol *75*, 1455-1467.
Sangurdekar, D.P., Zhang, Z., and Khodursky, A.B. (2011). The association of DNA damage response and nucleotide level modulation with the antibacterial mechanism of the anti-folate drug trimethoprim. BMC genomics *12*, 583.
Sliusarenko, O., Heinritz, J., Emonet, T., and Jacobs-Wagner, C. (2011). High-throughput, subpixel precision analysis of bacterial morphogenesis and intracellular spatio-temporal dynamics. Mol Microbiol *80*, 612-627.
Sperber, A.M., and Herman, J.K. (2017). Metabolism Shapes the Cell. J Bacteriol *199*.
Tamer, Y.T., Gaszek, I.K., Abdizadeh, H., Batur, T.A., Reynolds, K.A., Atilgan, A.R., Atilgan, C., and Toprak, E. (2019). High-Order Epistasis in Catalytic Power of Dihydrofolate Reductase Gives Rise to a Rugged Fitness Landscape in the Presence of Trimethoprim Selection. Mol Biol Evol *36*, 1533-1550.
Toprak, E., Veres, A., Michel, J.B., Chait, R., Hartl, D.L., and Kishony, R. (2012). Evolutionary paths to antibiotic resistance under dynamically sustained drug selection. Nat Genet *44*, 101-105.
Vadia, S., and Levin, P.A. (2015). Growth rate and cell size: a re-examination of the growth law. Curr Opin Microbiol *24*, 96-103.
Weart, R.B., Lee, A.H., Chien, A.C., Haeusser, D.P., Hill, N.S., and Levin, P.A. (2007). A metabolic sensor governing cell size in bacteria. Cell *130*, 335-347.
Wei, Y., Havasy, T., McPherson, D.C., and Popham, D.L. (2003). Rod shape determination by the Bacillus subtilis class B penicillin-binding proteins encoded by pbpA and pbpH. J Bacteriol *185*, 4717-4726.
Young, K.D. (2006). The selective value of bacterial shape. Microbiol Mol Biol Rev *70*, 660-703.

Zaritsky, A., and Pritchard, R.H. (1973). Changes in cell size and shape associated with changes in the replication time of the chromosome of Escherichia coli. Journal of bacteriology *114*, 824-837.
Zaritsky, A., Woldringh, C.L., Einav, M., and Alexeeva, S. (2006). Use of thymine limitation and thymine starvation to study bacterial physiology and cytology. J Bacteriol *188*, 1667-1679.

Figure 1

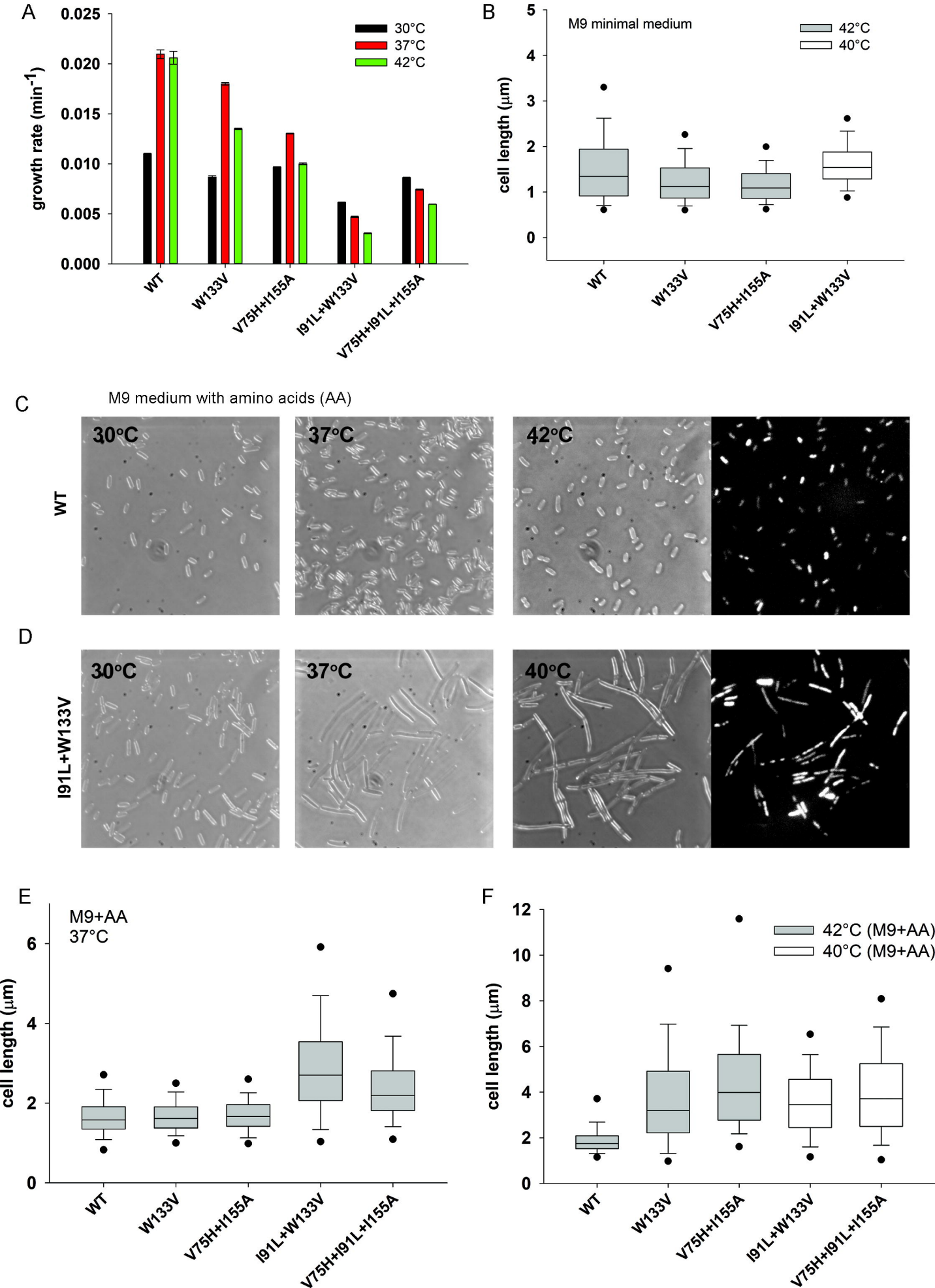
A
growth rate (min-1)
0.025
0.020
0.015
0.010
0.005
0.000
30°C
37°C
42°C
WT
W133V
V75H+I155A
I91L+W133V
V75H+I91L+I155A
B
M9 minimal medium
cell length (μm)
42°C
40°C
C
M9 medium with amino acids (AA)
WT
30°C
37°C
42°C
D
I91L+W133V
30°C
37°C
40°C
E
M9+AA
37°C
cell length (μm)
F
42°C (M9+AA)
40°C (M9+AA)

Figure 2

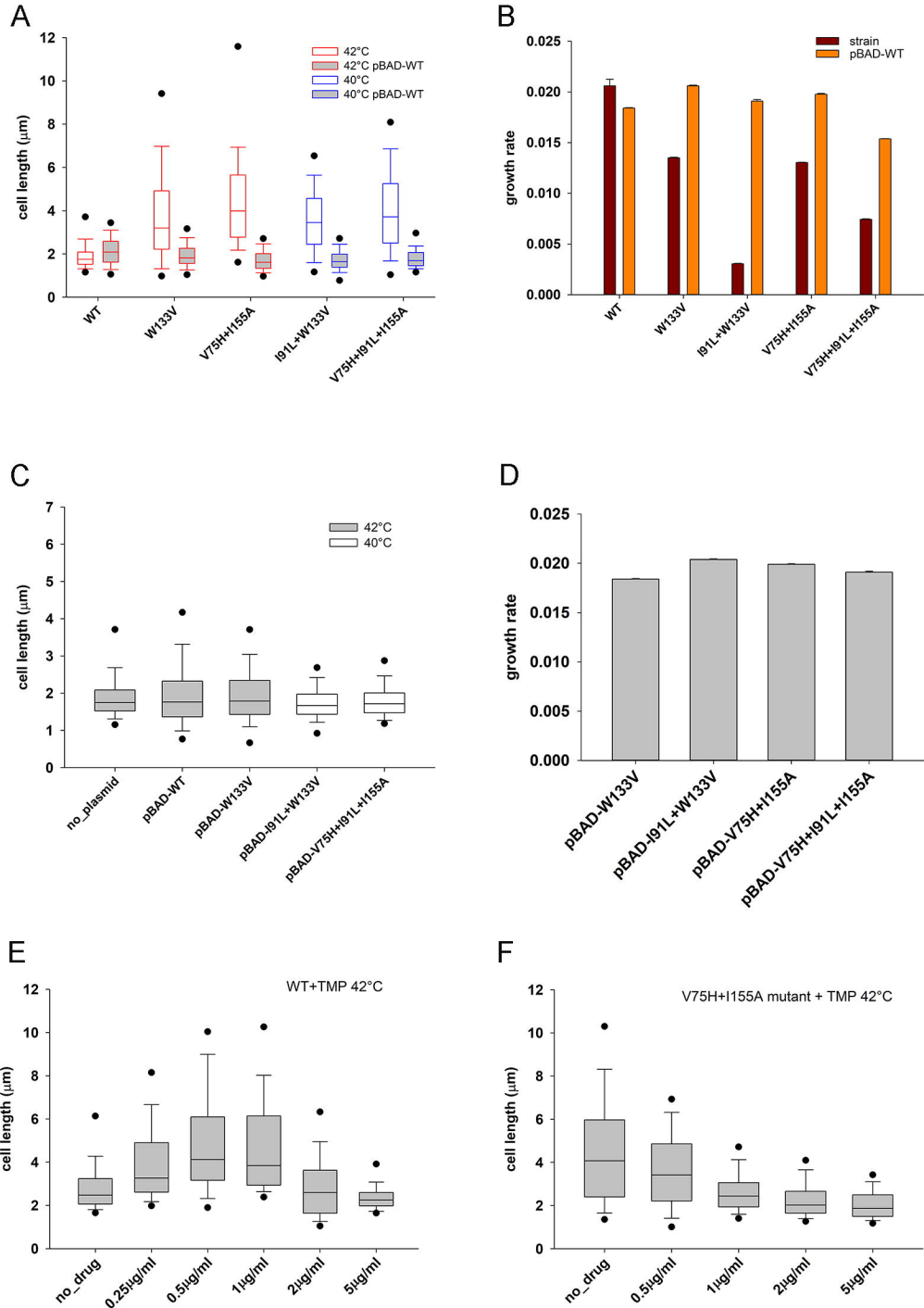
A
cell length (μm)
42°C
42°C pBAD-WT
40°C
40°C pBAD-WT
WT
W133V
V75H+I155A
I91L+W133V
V75H+I91L+I155A
B
growth rate
strain
pBAD-WT
WT
W133V
I91L+W133V
V75H+I155A
V75H+I91L+I155A
C
cell length (μm)
42°C
40°C
no_plasmid
pBAD-WT
pBAD-W133V
pBAD-I91L+W133V
pBAD-V75H+I91L+I155A
D
growth rate
pBAD-W133V
pBAD-I91L+W133V
pBAD-V75H+I155A
pBAD-V75H+I91L+I155A
E
WT+TMP 42°C
cell length (μm)
no_drug
0.25μg/ml
0.5μg/ml
1μg/ml
2μg/ml
5μg/ml
F
V75H+I155A mutant + TMP 42°C
cell length (μm)
no_drug
0.5μg/ml
1μg/ml
2μg/ml
5μg/ml

Figure 3

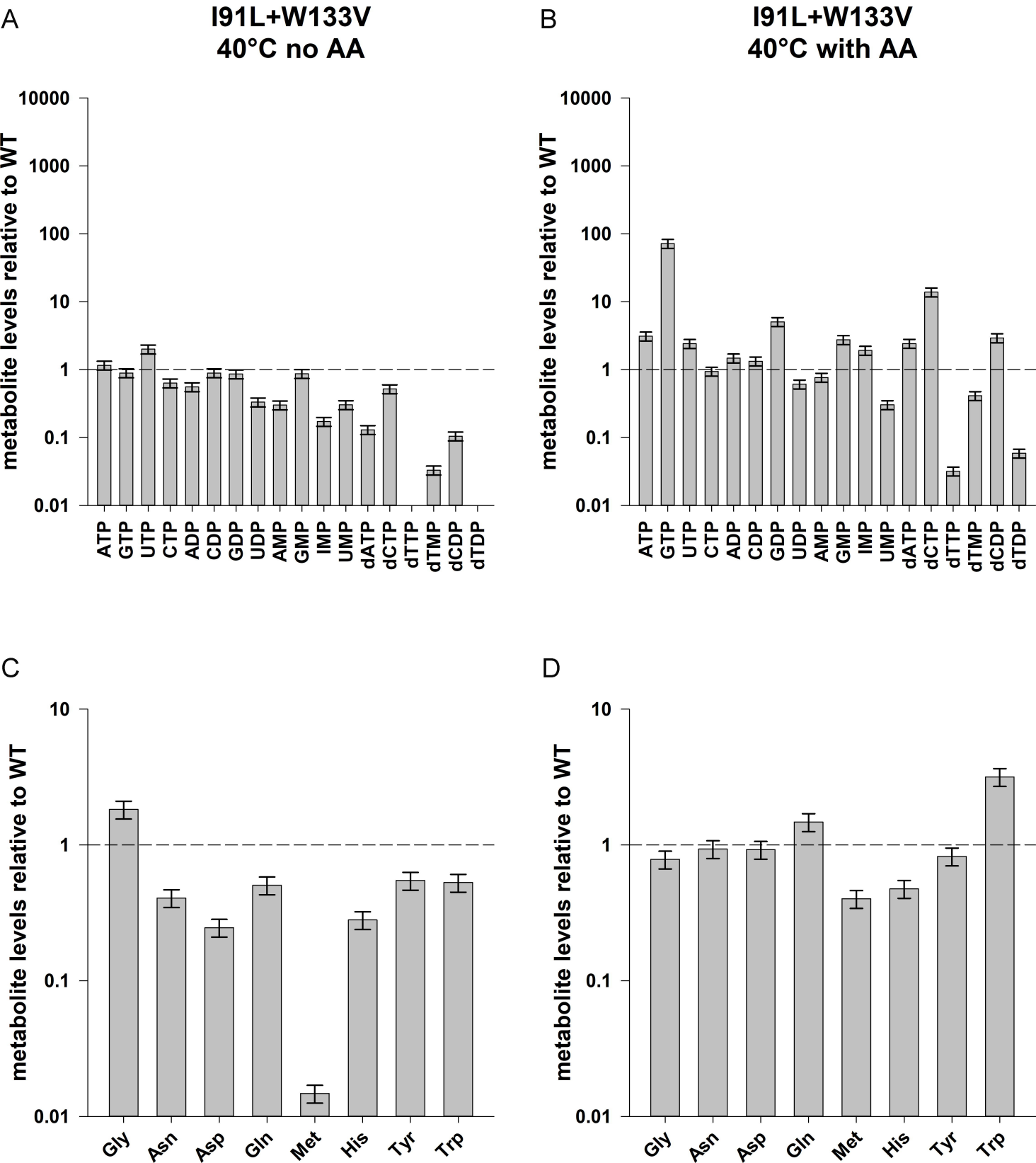
A
I91L+W133V
40°C no AA
B
I91L+W133V
40°C with AA
metabolite levels relative to WT
10000
1000
100
10
1
0.1
0.01
ATP
GTP
UTP
CTP
ADP
CDP
GDP
UDP
AMP
GMP
IMP
UMP
dATP
dCTP
dTTP
dTMP
dCDP
dTDP
C
D
Gly
Asn
Asp
Gln
Met
His
Tyr
Trp

Figure 4

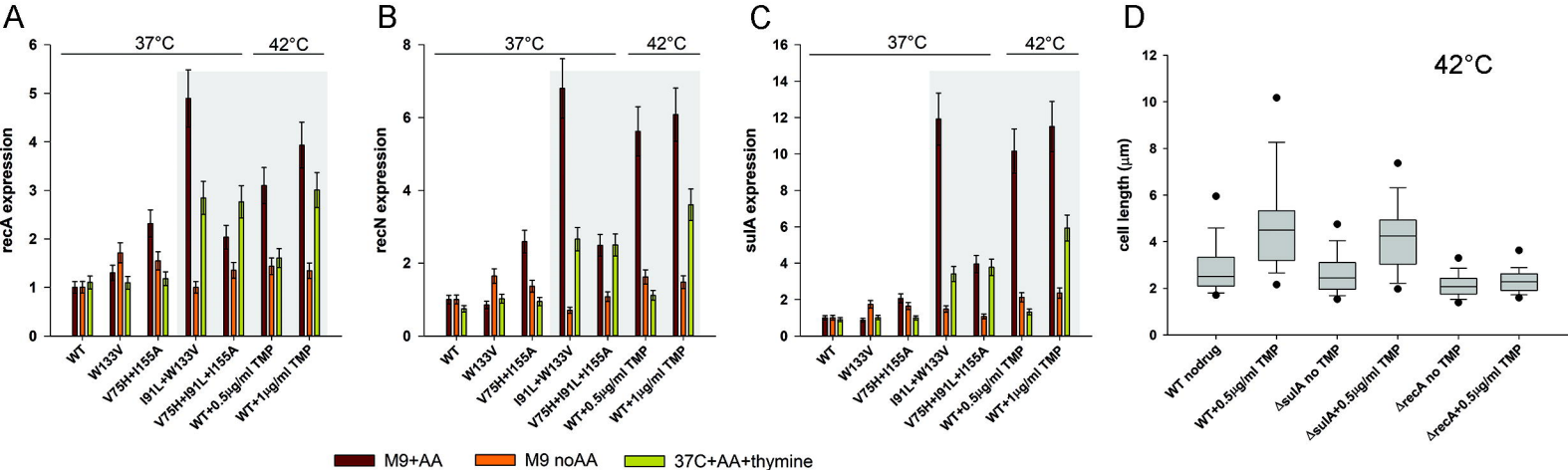
A
37°C
42°C
recA expression
0
1
2
3
4
5
6
WT
W133V
V75H+I155A
I91L+W133V
V75H+I91L+I155A
WT+0.5μg/ml TMP
WT+1μg/ml TMP
B
37°C
42°C
recN expression
0
2
4
6
8
WT
W133V
V75H+I155A
I91L+W133V
V75H+I91L+I155A
WT+0.5μg/ml TMP
WT+1μg/ml TMP
C
37°C
42°C
sulA expression
0
2
4
6
8
10
12
14
16
WT
W133V
V75H+I155A
I91L+W133V
V75H+I91L+I155A
WT+0.5μg/ml TMP
WT+1μg/ml TMP
D
42°C
cell length (μm)
0
2
4
6
8
10
12
WT nodrug
WT+0.5μg/ml TMP
ΔsulA no TMP
ΔsulA+0.5μg/ml TMP
ΔrecA no TMP
ΔrecA+0.5μg/ml TMP
M9+AA
M9 noAA
37C+AA+thymine

Figure 5

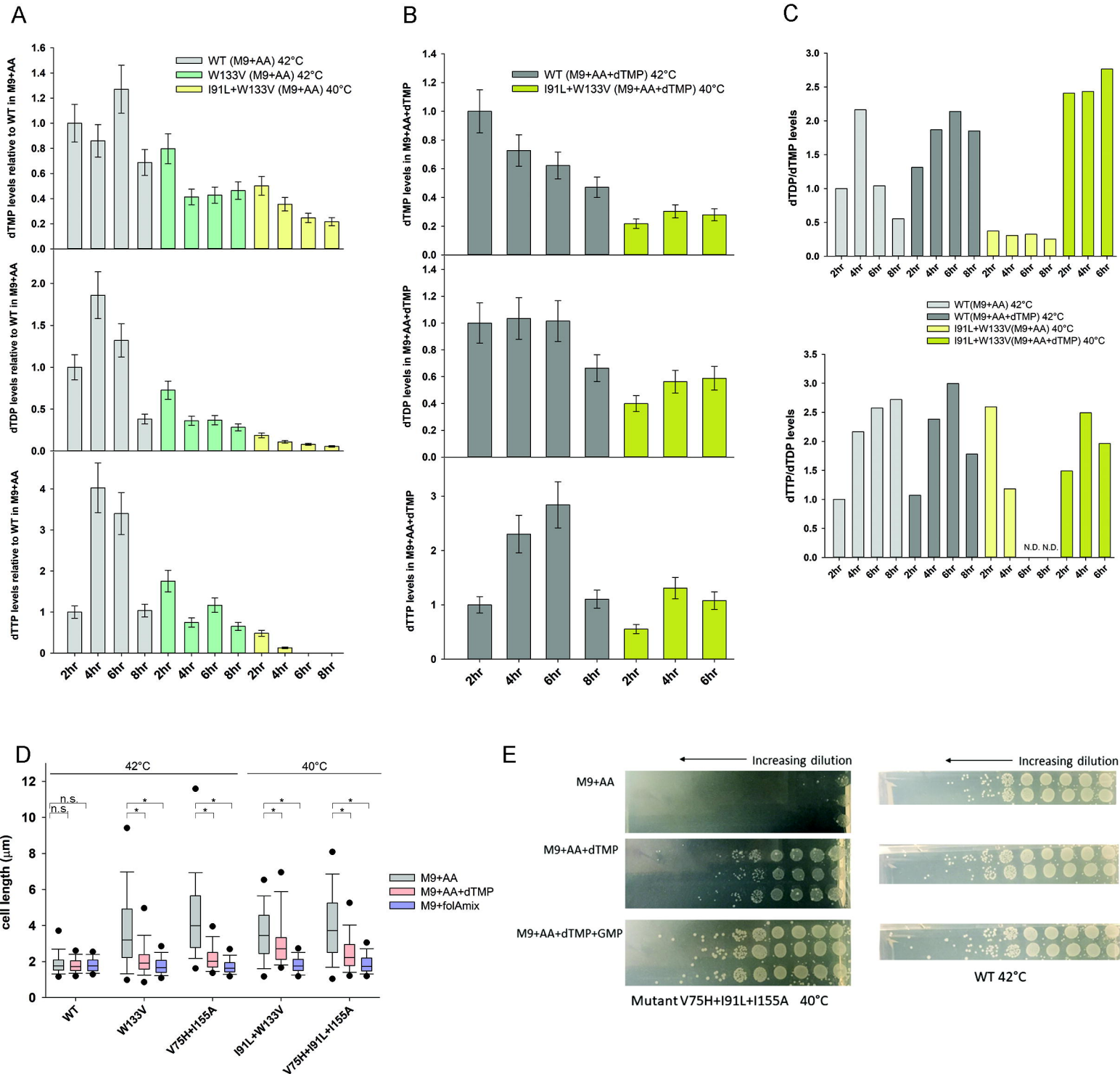
A
WT (M9+AA) 42°C
W133V (M9+AA) 42°C
I91L+W133V (M9+AA) 40°C
dTMP levels relative to WT in M9+AA
dTDP levels relative to WT in M9+AA
dTTP levels relative to WT in M9+AA
2hr 4hr 6hr 8hr 2hr 4hr 6hr 8hr 2hr 4hr 6hr 8hr
B
WT (M9+AA+dTMP) 42°C
I91L+W133V (M9+AA+dTMP) 40°C
dTMP levels in M9+AA+dTMP
dTDP levels in M9+AA+dTMP
dTTP levels in M9+AA+dTMP
2hr 4hr 6hr 8hr 2hr 4hr 6hr
C
dTDP/dTMP levels
dTTP/dTDP levels
WT(M9+AA) 42°C
WT(M9+AA+dTMP) 42°C
I91L+W133V(M9+AA) 40°C
I91L+W133V(M9+AA+dTMP) 40°C
N.D. N.D.
D
42°C
40°C
n.s.
cell length (μm)
M9+AA
M9+AA+dTMP
M9+folAmix
WT
W133V
V75H+I155A
I91L+W133V
V75H+I91L+I155A
E
Increasing dilution
M9+AA
M9+AA+dTMP
M9+AA+dTMP+GMP
Mutant V75H+I91L+I155A 40°C
WT 42°C

Figure 6

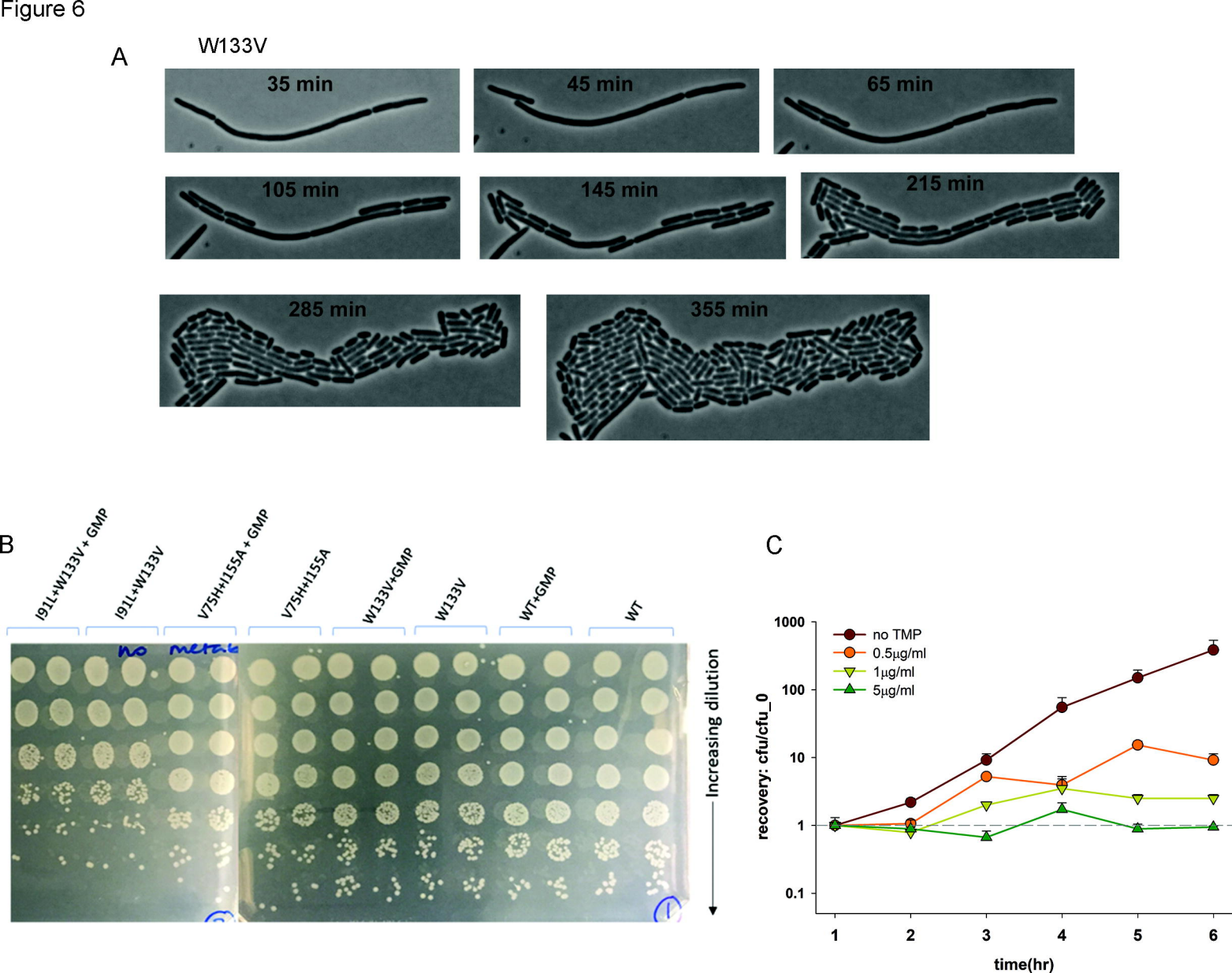
A
W133V
35 min
45 min
65 min
105 min
145 min
215 min
285 min
355 min
B
I91L+W133V + GMP
I91L+W133V
V75H+I155A + GMP
V75H+I155A
W133V+GMP
W133V
WT+GMP
WT
no metal
Increasing dilution
C
no TMP
0.5μg/ml
1μg/ml
5μg/ml
recovery: cfu/cfu_0
1000
100
10
1
0.1
1
2
3
4
5
6
time(hr)

Figure 7

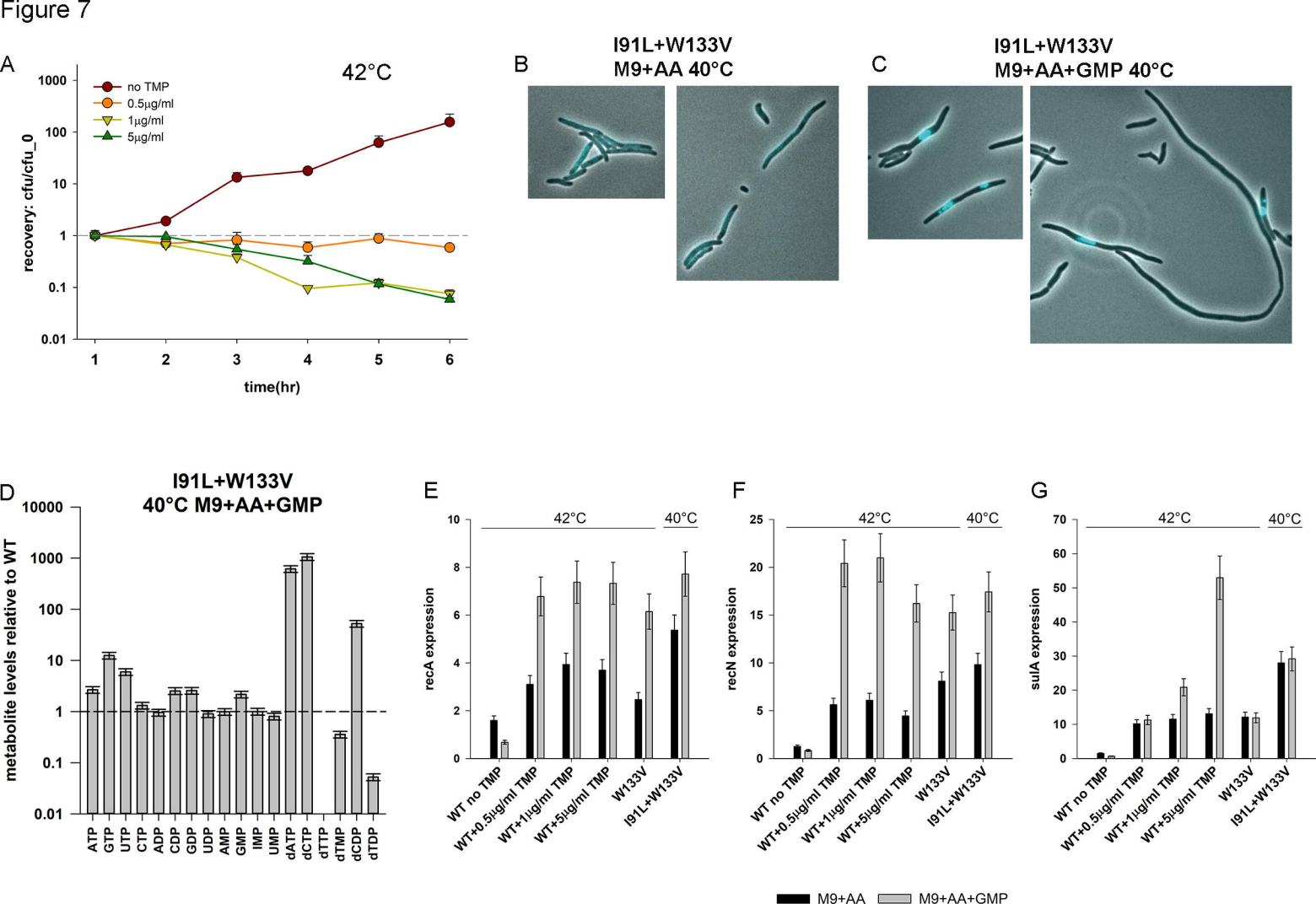
A
42°C
no TMP
0.5μg/ml
1μg/ml
5μg/ml
recovery: cfu/cfu_0
time(hr)
B
I91L+W133V
M9+AA 40°C
C
I91L+W133V
M9+AA+GMP 40°C
D
I91L+W133V
40°C M9+AA+GMP
metabolite levels relative to WT
ATP
GTP
UTP
CTP
ADP
CDP
GDP
UDP
AMP
GMP
IMP
UMP
dATP
dCTP
dTTP
dTMP
dCDP
dTDP
E
recA expression
F
recN expression
G
sulA expression
42°C
40°C
WT no TMP
WT+0.5μg/ml TMP
WT+1μg/ml TMP
WT+5μg/ml TMP
W133V
I91L+W133V
M9+AA
M9+AA+GMP